Groundwater promotes emergence of asporogenic mutants of emetic Bacillus cereus

Ludivine Rousset, Béatrice Alpha-Bazin, Alice Chateau, J. Armengaud, Thierry Clavel, Odile Berge, Catherine Duport

Groundwater promotes emergence of asporogenic mutants of emetic *Bacillus cereus*

Ludivine Rousset[1,3], Béatrice Alpha-Bazin[2], Alice Chateau[1], Jean Armengaud[2], Thierry Clavel[1], Odile Berge[3] and Catherine Duport*[1]

[1] Avignon Université, INRAE, UMR SQPOV, F-84914, Avignon, France

[2] Université Paris Saclay, CEA, INRAE, Département Médicaments et Technologies pour la Santé (DMTS), SPI, 30200 Bagnols-sur-Cèze, France.

[3]INRAE, Pathologie Végétale, F-84140, Montfavet, France.

*Corresponding author: Pr. Catherine Duport

Address: Avignon Université, INRAE, UMR SQPOV, F-84914, Avignon, France.

E-mail: catherine.duport@univ-avignon.fr.

Phone: +33 432 722 507

Running tittle: *B. cereus* survival in groundwater

This article has been accepted for publication and undergone full peer review but has not been through the copyediting, typesetting, pagination and proofreading process which may lead to differences between this version and the Version of Record. Please cite this article as doi: 10.1111/1462-2920.15203

Originality-Significance Statement

This work reports for the first time that asporogenic mutants of *Bacillus cereus* accumulate in a natural oligotrophic medium. As groundwater is used to irrigate food crops, and *B. cereus* is a food-borne pathogen, these findings are highly significant for human health.

Summary

Bacillus cereus is a ubiquitous endospore-forming bacterium, which mainly affects humans as a food-borne pathogen. *B. cereus* can contaminate groundwater used to irrigate food crops. Here, we examined the ability of the emetic strain *B. cereus* F4810/72 to survive abiotic conditions encountered in groundwater. Our results showed that vegetative *B. cereus* cells rapidly evolved in a mixed population composed of endospores and asporogenic variants bearing *spo0A* mutations. One asporogenic variant, VAR-F48, was isolated and characterized. VAR-F48 can survive in sterilized groundwater over a long period in a vegetative form, and has a competitive advantage compared to its parental strain. Proteomics analysis allowed us to quantify changes to cellular and exoproteins after 24 and 72 h incubation in groundwater, for VAR-F48 compared to its parental strain. The results revealed a significant rerouting of the metabolism in the absence of Spo0A. We concluded that VAR-F48 maximizes its energy use to deal with oligotrophy, and the emergence of *spo0A*-mutated variants may contribute to the persistence of emetic *B. cereus* in natural oligotrophic environments.

Introduction

Groundwater accounts for most of the liquid fresh water on earth. It is the greatest water resource for humans and is increasingly used to irrigate food crops and to wash vegetables (Siebert et al., 2010). Water from underground aquifers is often considered to be of better microbiological quality than surface water, as it has undergone natural filtration as it percolated through the overlying layers of soil (John and Rose, 2005; Dillon et al., 2008). However, food borne pathogens such as *Bacillus cereus* have been isolated from groundwater in viable and cultivable forms (Brillard et al., 2015).

B. cereus is a soil-borne, endospore-forming, Gram-positive bacterium. It is transported from soil into the groundwater by leaching (Brillard et al., 2015). Leaching is increased by heavy rainfall and intensive irrigation, both of which will increase with global warming (Zhou et al., 2010; Green and Anapalli, 2018; Saleem et al., 2020). In addition to increasing the flow of water through the soil, global warming may affect the diversity of bacteria (Classen et al., 2015). In the case of *B. cereus*, it could contribute to increase the population of pathogenic mesophilic strains in the soil (Carlin et al., 2010), and consequently in groundwater. It raises the question of the health risks associated with groundwater contamination. The health risks depend on the size of the inoculum, but also on the ability of *B. cereus* to survive the hostile abiotic conditions encountered in groundwater. These conditions include a relatively low temperature (16 °C) and low levels of available organic matter (Rousset et al., 2019). *B. cereus* is a facultative anaerobic chemoorganotroph, capable of both respiratory and fermentative metabolism (Rosenfeld et al., 2005; Duport et al., 2006), and not an oligotroph *per se, i.e.*, capable of growing under conditions of extreme energy or/and nutrient limitation

(Lever et al., 2015). However, it has a considerable capacity for metabolic adaptation, allowing it to survive and grow under various stress conditions, affording it a considerable pathogenic potential (Duport et al., 2016).

B. cereus causes food-borne diseases primarily characterized by emetic or diarrheal syndromes. Diarrheal syndromes are thought to be caused by ingestion of *B. cereus* cells and / or spores, which can then produce Hemolysin BL (HBL), Non-hemolytic enterotoxin (Nhe) and/or Cytotoxin K (CytK) in the intestine (Stenfors Arnesen et al., 2008; Jessberger et al., 2015). However, *B. cereus* also produces several other proteins with toxic effects *in vitro* or in animal models, and some of them may also contribute to symptoms in these syndromes (Ramarao and Sanchis, 2013). Emetic syndromes, in contrast, are caused directly by the ingestion of a toxin, cereulide, produced by *B. cereus* as it grows in food (Agata et al., 2002).

B. cereus is part of a group of closely related species and lineages, including *Bacillus anthracis*, *Bacillus cytotoxicus*, *Bacillus mycoides*, *Bacillus pseudomycoides*, *Bacillus thuringiensis*, *Bacillus toyonensis*, and *Bacillus weihenstephanensis*, which in the literature is often referred to as *Bacillus cereus sensu lato* (Drobniewski, 1993; Guinebretiere et al., 2013; Pfrunder et al., 2016; Liu et al., 2017; Ehling-Schulz et al., 2019; Carroll et al., 2020). Previous studies have divided *B. cereus s.l.* into seven major phylogenetic groups (Guinebretiere et al., 2008; Guinebretiere et al., 2010), several of which contain strains known colloquially as "*B. cereus*". The seven genetic groups have different thermal adaptive capacities, and varying degrees of association with health risks (Guinebretiere et al., 2008; Carroll et al., 2019; Ehling-Schulz et al., 2019). Group III is often regarded as a high-health risk group, as it contains *B.*

cereus s.l. strains capable of causing anthrax or emetic illness (Guinebretiere et al., 2008; Kolsto et al., 2009; Guinebretiere et al., 2010).

In this study, we investigated the ability of the emetic reference *B. cereus* strain F4810/72 (also named AH187) to survive long-term under extreme nutrient and energy deprivation, mirroring the abiotic conditions encountered in natural groundwater. Incubating vegetative *B. cereus* F4810/72 cells in groundwater at 16 °C resulted in selection of asporogenic *spo0A* mutants. Relative quantitative proteomics analyses were used to compare the protein profile of the parental strain and a *spo0A*-mutated variant. Results indicated that emerging mutants expressed the Growth Advantage in Stationary Phase (GASP) phenotype.

Results

Survival of B. cereus F4810/72 in groundwater generates a mixed population with normal and atypical colony morphologies

B. cereus survival was studied in sterilized groundwater under physicochemical conditions designed to mimic natural conditions (16 °C under agitation; (Rousset et al., 2019)). Figure 1A shows a biphasic decay profile of viable cells over 30 days. Accordingly, data were best fit by the biphasic model using the GInaFiT freeware modeling tool (Geeraerd et al., 2005). The specific rate of decay is 1.47 ± 0.65 day^{-1} in the first fast phase and is related to 91± 5% of the initial population, while the specific decay rate is 0.04 ± 0.02 day^{-1} in the second slow phase (Fig. 2). After 3 days' incubation, which corresponds to the end of the first decay phase, almost all viable cells (4.2 ± 0.6 log CFU) were recovered as heat-resistant endospores (4.3 ± 0.8 log CFU), whereas after 30 days, only 16.8 ± 4.5 % of the viable cells were recovered as heat-

resistant endospores. Spores therefore germinated in groundwater (Brillard et al., 2015). Heat-treated culture samples formed uniform colonies on LB agar plates (data not shown). However, colony heterogeneity, with colonies differing in size and appearance, was observed with untreated samples after 6 days' incubation in groundwater (Fig. 1B). The differences in appearance between atypical and standard colonies were further enhanced by the addition of Congo Red (Fig. 1C), suggesting that the *B. cereus* population contained both WT and variant bacteria (Worsham and Sowers, 1999). Fig. 1A shows that morphological variants quickly accumulated over 8 days and constituted the main population after 30 days (91.8 ± 6.0 %), replacing heat-resistant endospores. Accumulation of variants was not due to contamination of the stock strain (data not shown). Taken together, these data suggest that spore germination can promote the emergence of variants in groundwater. However, we cannot exclude the possibility that very few vegetative cells mutated and became non-sporulating cells.

To determine whether the enrichment of morphological variants was a result of nutrient deficiency, we compared the dynamics of *B. cereus* populations grown in groundwater and MOD_{50} medium (Rosenfeld et al., 2005). Variants accumulated 20 days earlier in oligotrophic groundwater than in minimal MOD_{50} medium (data not shown), suggesting that extreme nutrient deficiency accelerates the emergence of morphological *B. cereus* variants.

Genetic analysis of morphological variants

To determine whether these morphological variants shared characteristics, we isolated 12 distinct variants from four independent experiments. Morphological differences were maintained for all of them and were stable following subculture in LB (data not shown). We

then tested the capacity of bacteria to form heat-resistant endospores in Fortified Nutrient Agar (FNA (Gonzalez et al., 1995)). The proportion of heat-resistant colonies obtained after 5 days' incubation was 0.1± 0.2%, indicating that morphological variants are asporogenic bacteria. Since the variant phenotype was irreversible, it could result from loss of endogenous plasmids or gene mutations, especially in the gene encoding the sporulation response regulator Spo0A that mutates predominantly in *B. anthracis* (Sastalla and Leppla, 2012).

To test the first hypothesis, PCR assays amplifying each of the four endogenous plasmids present in F4810/72 were performed. PCR products for WT and variant strains were identical, indicating that variants had conserved all four plasmids (data not shown).

We next tested the gene mutation hypothesis by amplifying and sequencing the *spo0A* gene. Strikingly, all of the selected variants contained a mutation in *spo0A*, with a different mutant subpopulation in each experiment (data summarized in Fig. S1). Closer analysis of *spo0A* sequences revealed the following four genetic variations (Fig. S1): (1) insertion of GA at position 700 of the *spo0A* ORF, resulting in truncation of 11 amino acids in Spo0A; (2) a nonsynonymous (C→T) mutation at position 563 resulting in an Ala→Val alteration; (3) a nonsynonymous (C→T) mutation at position 667 changing Arg→Cys; (4) a synonymous (G→A) mutation at position 39.

The first three variations could clearly alter the primary structure of the Spo0A protein and thus, may cause a sporulation deficiency in variants. A synonymous mutation, on principle, does not alter the protein's structure, but it may alter the structure and function of the mRNA (Lebeuf-Taylor et al., 2019). To determine whether the synonymous mutation detected in the VAR-F48 subpopulation variant is the genetic determinant of the sporulation deficiency observed, its

whole genome was sequenced. This analysis revealed two additional non-synonymous mutations, at positions 3 797 954 and 2 222 681 (nucleotide locations are in reference to the *B. cereus* AH187 genome sequence, NCBI RefSeq Accession NC_011658.1). These mutations respectively altered codon 178 of *ctaA* (GCT→ACT, Ala→Thr), encoding heme A synthase, and codon 49 of the BCAH187_A2382 gene (CAC→CAG, His→Asp), encoding a protein of unknown function (Fig. S1). Thus, the asporogenic phenotype of VAR-F48 cannot be linked solely to the nonsynonymous mutation identified in *spo0A*.

Survival of the asporogenic VAR-F48 strain in groundwater

Genetic variants are generally adapted to the environment where they evolved, so to determine whether VAR-F48 has a distinct advantage over the WT strain in groundwater, we examined its survival alongside that of the WT parental strain. The survival kinetics of the two strains were compared using the biphasic model (Fig. 2). The data show that the specific rate of decay of VAR-F48 was lower in the first fast phase and higher in the second slow phase (0.54±0.20 day^{-1} and 0.14±0.06 day^{-1}, respectively) compared to WT. As a result, the reduction rate reached 3.5 log in 30 days for VAR-F48 cells while it reached 1.5 log reduction for WT cells. Finally, although VAR-F48 can survive for 30 days in groundwater, its survival rate was lower than that of its parent.

Cellular proteome analysis provides clues to survival of asporogenic VAR-F48 in groundwater

To further investigate the molecular mechanisms used by VAR-F48 to survive in groundwater, we compared the cellular proteomes of asporogenic VAR-F48 and endospore-forming WT after

incubation in groundwater for 24 h (T1) and 72 h (T2) (Fig. S2). The inoculum (T0) was exponentially growing cells cultivated in MOD_{50} medium (Rosenfeld et al., 2005), which were harvested at maximal growth rate (μ_{max}). Interestingly, the μ_{max} for VAR-F48 (0.15±0.05 h^{-1}) was higher than that for WT (0.09±0.01 h^{-1}), indicating that VAR-F48 grows faster than WT in nutrient-replete medium.

Shotgun proteomics analysis was performed on three biological replicates for each strain at each of the three time-points. In total, 2184 cellular proteins were identified by at least two distinct peptides across all 18 samples analyzed (Table S1). Principal Component Analysis (PCA) was performed on normalized data. An adjusted *p*-value <0.05 and a $|\text{fold-change}| \geq 1.5$ were required in at least one pairwise comparison across the dataset (Fig. 3A). This analysis revealed good homogeneity of the replicates at each time-point, and clear segregation between VAR-F48 and WT samples. PCA also indicated that VAR-F48 samples collected after 24 h and 72 h converged, whereas WT samples segregated in a time-dependent manner. This observation indicates that proteome remodeling occurring in VAR-F48 differed from that occurring in the WT strain, and that this remodeling may be completed earlier in VAR-F48. All possible pairwise comparisons to identify proteins that were differentially accumulated (DAPs) between VAR-F48 and WT samples at the same time points were carried out to identify protein profiles specifically associated with VAR-F48 survival (Table S2). Overall, 296 DAPs were identified, how they overlap at the three time points is illustrated in Fig. 3B. Three main groups of differentially abundant proteins were distinguished: (1) those that are common to T0, T1 and T2; (2) those that are common to T1 and T2; and (3) those that are specific to each time-point.

Group 1: this group includes 14 proteins that differentially accumulated in VAR-F48 compared to WT both in MOD_{50} medium (inoculum, T0) and in groundwater after 24 h (T1) and/or 72 h (T2) incubation. Therefore, the genetic background probably contributes to enrichment or depletion of these proteins in VAR-F48. Of these 14 proteins, four were more abundant in VAR-F48 compared to WT, and ten were produced at lower levels in VAR-F48 than in WT (Table 1).

Among the enhanced-DAP, we found a lactate dehydrogenase (LDH), which regenerates NAD^+ from NADH, with concomitant reduction of pyruvate to lactate to regulate overflow metabolism under aerobiosis; a flavohemoprotein (Hmp), which is known to protect bacteria from endogenous redox stress (Moore et al., 2004); and a component of the thiamine pyrophosphate biosynthesis pathway (ThiS). Thiamine pyrophosphate is an important co-factor for several enzymes involved in energy metabolism, and might be involved in the adaptation of bacteria to energy stress (Gigliobianco et al., 2010). Taken together, these proteins reflect changes to energy/redox metabolic mechanisms. Among the proteins that were less abundant in VAR-F48 than in WT, two (CesC and CesD) are essential for posttranslational control of cereulide synthesis (Lucking et al., 2015). In addition, EA1, which is known to self-assemble into a paracrystalline layer on the surface of bacilli, was undetectable in VAR-F48 at any of the three time points (Table 1). In *B. anthracis*, both EA1 and Sap can self-assemble (Kern et al., 2012). *B. cereus* AH187 synthesizes a protein (B7HXP4), which resembles Sap. Like EA1, B7HXP4 was identified as a decreased-DAP, and was not detected in VAR-F48. The final protein in this subgroup is Spo0A, which was also undetectable in VAR-F48 (Table 1). This result suggests that VAR-F48 does not synthetize Spo0A due to the *spo0A* mutation. To confirm

this finding, we analyzed the proteome of VAR-F48 grown in LB medium; Spo0A, EA1, B7HPX4, and Ces proteins were also undetectable in these conditions (data not shown; confirmed by Western-blot, Fig. 6).

Group 2. This group consisted of 16 proteins that differentially accumulated persistently after 24 h incubation in groundwater. These proteins may thus be key components of the sustained molecular response to the stress conditions encountered in groundwater.

Of the 16 DAPs, thirteen were detected at higher abundance, and three at lower abundance in VAR-F48 compared to WT (Table 2). Of the 13 enhanced-DAPs, eight were assigned to central metabolic pathways, one was predicted to be a signal sensor, and one corresponded to Catabolite Control Protein A (CcpA). CcpA is a pleiotropic transcriptional regulator involved in the general mechanisms controlling carbon catabolite repression (Gorke and Stulke, 2008). The decreased-DAPs included sigma factor E (σ^E), which drives sporulation in Bacilli (Fimlaid and Shen, 2015), and the sporulation-associated protein CotE. Taken together, these data indicate that VAR-F48 enters into an active survival process, which is distinct from the sporulation process.

Group 3. This group includes transient DAPs that could reflect the metabolic status of VAR-F48 in nutrient-replete inoculum (subgroup T0) and in nutrient-depleted groundwater after 24 h (subgroup T1) and 72 h incubation (subgroup T2).

Subgroup T0. Of the 157 DAPs identified only at T0, expression of 61 was enhanced and of 96 was decreased in VAR-F48 compared to WT, indicating a general down-regulation of protein expression in VAR-F48 compared to WT. We classified DAPs according to Clusters of Orthologous Groups (COG) groupings (Table S2), and Figure 4 (T0) shows the distribution of

the 53 enhanced-DAPs and 71 decreased-DAPs that were functionally categorized. The data indicate that proteins related to lipid transport and metabolism, and to a lesser extent, amino acid or nucleotide transport and metabolism, were expressed at lower levels in VAR-F48. In contrast, proteins related to coenzyme transport, general metabolism, and defense mechanisms were expressed at higher levels in VAR-F48. Of the 12 decreased-DAPs in the lipid group, five were annotated as acetyl-CoA dehydrogenases, three were acetyl-CoA synthases, and two were enoyl-CoA hydratases. This profile suggests a reduced need for fatty acid oxidation as energy source in VAR-F48 compared to WT. In the amino acid-related group, proteins that were less abundant in VAR-F48 tended to be involved in biosynthesis pathways, including those for His, Leu, Met, Ile, and Phe. Interestingly, one of the five decreased-DAPs in the nucleotide-related category was annotated as a RelA-SpoT domain-containing protein (B7HPP2), and may be involved in the stringent response (Pulschen et al., 2017). Its low level in VAR-F48 compared to WT (log_2 fold-change = -3.18) suggests that nutritional status was detected differently by VAR-F48 and WT strains. In the coenzyme-related category, the nine enhanced-DAPs were related to thiamine biosynthesis (B7HWF0, ThiD1 and ThiM), molybdate insertion (B7HPA9, B7HPB0), iron transport (B7HWD6, B7HZS9), and cobalamin synthesis (B7HPB8). The four enhanced-DAPs classed in the defense group, were catalase (KatB), Organic hydroperoxide resistance protein (Ohr), DNA protection during starvation protein 2 (Dps2), and nitric oxide synthase oxygenase (NOS), all of which are involved in the redox/oxidative stress response (Clair et al., 2013; Holden et al., 2013; Shu et al., 2013). Figure 4 (T0) also shows that in carbohydrate, energy, transport, transcription, and pathogenesis-related categories, the numbers

of enhanced- and decreased-DAPs were almost the same. We examined these categories in detail to detect possible metabolic shifts (Table S2).

(i) In the carbohydrate-related category, enhanced levels of pyruvate formate lyase (Pfl, B7HU44), pyruvate formate lyase activating enzyme (PflA, B7HU45) and alcohol dehydrogenase (Adh, B7HQ62) were associated with decreased levels of TCA enzymes citrate synthase (B7HR26) and isocitrate lyase (B7HZQ5), suggesting that anaerobic catabolic pathways may be induced at the expense of aerobic catabolic pathways in VAR-F48. In addition, enhanced levels of glucose-specific IIABC components of the Phosphotransferase system (PtsG) and glyceraldehyde-3-phosphate dehydrogenase (GapN) may support increasing glycolysis in VAR-F48, and increased expression of lactate utilization proteins A and B (LutA, LutB) may support the use of excreted lactate as carbon source.

(ii) In the energy-related category, four out of seven enhanced-DAPs were components of the respiratory nitrate reductase (NarGHIJ) and two are components of nitrite reductase (NirB, NirD). Among the decreased-DAPs, two were components of the respiratory menaquinone-cytochrome *c* reductase complex (QcrA, QcrC) and two were Etf electron transferring flavoprotein enzymes (EtfA, EtfB). Etfs are known to transfer electrons from a variety of fatty acid or amino acid substrates into the respiratory electron transport chain via an Etf-quinone oxidoreductase and the reduced quinone pool (Garcia Costas et al., 2017). Taken together, these data suggest that the electron transfer process is altered in VAR-F48 compared to WT.

(iii) In the pathogenesis-related group, we noted enhanced expression of NheA and NheB, components of the Nhe enterotoxin, and of the Immune Inhibitor A metalloprotease InhA1. In contrast, the CesA and CesT components of cereulide synthetase were less abundant. This

profile indicates that the VAR-F48 background favors enterotoxins and InhA1 synthesis at the expense of cereulide in growing cells. Finally, the comparative analysis suggested multiple changes in metabolic pathways that are involved in maintaining redox and energy homeostasis, under stress conditions.

Subgroup T1. The number of DAPs identified only at T1 was ~7-fold smaller than at T0, indicating a strong down-regulation of both proteomes after 24 h in groundwater. The majority (21 out 23) of T1-exclusive DAPs were proteins for which expression was enhanced in VAR-F48. One third of enhanced-DAPs were categorized in amino acid, and translation-related groups (Fig. 4 (T1)), indicating an active metabolism in VAR-F48. Interestingly, the protein with the highest abundance in VAR-F48 compared to WT (log_2 fold-change = 4.6) was the intron-containing RecA protein B7HLB3 (Ko et al., 2002), which was classed in the replication, recombination, and DNA repair COG category. RecA proteins play a central role in DNA stability and repair under stress conditions leading to DNA damage. Taken together, these data suggest that a significant fraction of energy expended by VAR-F48 after 24 h incubation in groundwater may be used to repair and replace damaged molecules.

Subgroup T2. Of the 68 DAPs identified only at T2, only 15 proteins were detected at higher levels in VAR-F48 compared to WT. These enhanced-DAPs were distributed across 10 functional groups (Fig. 4 (T2)) and include the universal stress protein B7HRR7 and the GTP binding protein Obg (B7HQJ8). Obg acts as an energy sensor to regulate essential cellular processes such as DNA replication and ribosome maturation, and it plays a key role in several stress-adaptation pathways such as the stringent response, and the general stress response (Kint et al., 2014). Obg is also necessary for the stress-induced activation of σB (Scott and

Haldenwang, 1999). Although the distribution of enhanced-DAPs within functional groups is relatively homogenous, a high proportion of decreased-DAPs (16) was classed in the sporulation group (SspB, GerQ, GerE, SasP1, B7HQI3, B7HNC6, SpoVFB, SpoIVA, B7HWM2, B7HT37, CotJC, SpoIIID, B7HUB9). This expression pattern suggests that WT actively entered sporulation after 72 h incubation in groundwater, whereas VAR-F48 underwent starvation and induced a nutrient/energy stress response.

Exoproteome analysis of asporogenic VAR-F48

We next compared the VAR-F48 and WT exoproteomes after 24 h (T1) and 72 h (T2)-incubation in groundwater. A total of 160 proteins were identified by at least two peptides (Table S3). Only 13 proteins were found to have differentially accumulated between the strains according to our quantitative and statistical criteria (Table S4). At T1, only two DAPs were identified, both were more abundant in VAR-F48 compared to WT. At T2, 11 DAPs were found, all less abundant in VAR-F48 compared to WT. These DAPs are mainly related to intracellular processes (Table 3), and consequently are not classical secreted proteins (Bendtsen et al., 2005).

Phenotypic characterization of asporogenic VAR-F48

Since biofilm formation and motility are important for bacterial survival, we tested the ability of VAR-F48 to produce biofilms using a crystal violet assay (Omer et al., 2015). We also tested the capacity of VAR-F48 to engage in swimming and swarming motility (Salvetti et al., 2007). No significant differences in biofilm formation were observed between VAR-F48

and the parental strain after 24 h and 48 h incubation (Fig. 5A). In contrast, biofilm production was higher in VAR-F48 than in WT after 72 h ($p<0.05$, according to unpaired two-tailed t-test), at which time WT cells were mainly present as endospores (data not shown). VAR-F48 showed a lower rate of swimming motility than WT (Fig. 5B, *p*-values associated with time, strain and time*strain factors in mixed model were all <0.05), but the two strains showed similar swarming rates (Fig. 5C). In summary, motility but not biofilm production capacity was altered in VAR-F48 compared to WT.

Complementation of the asporogenic VAR-F48 strain

CtaA is required for cytochrome *aa3* oxidase biosynthesis and sporulation in *Bacillus subtilis* (Mueller and Taber, 1989). Oxidase activity was detectable in both VAR-F48 and WT strains (data not shown). Neither colony morphology nor sporulation were restored following complementation of VAR-F48 with the recombinant replicative plasmid pHT304-*ctaA* (data not shown). In contrast, VAR-F48 transformed with pHT304-*spo0A* plasmids formed colonies with similar morphology to wild-type, and sporulated in FNA medium. In addition, deletion of BCAH187_A2382 gene did not impact *B. cereus* sporulation (data not shown). As compensation of the *ctaA* mutation did not restore sporulation, and the BCAH187_A2382 gene appeared to play no role in sporulation, these results indicate that the sporulation deficiency in VAR-F48 was due only to the *spo0A* mutation.

As *spo0A* regulates the S-layer protein gene *sap* in *B. anthracis* (Plaut et al., 2014), we next wished to determine whether s*po0A* complementation could restore both S-layer protein synthesis and Spo0A synthesis. To do so, we extracted proteins from cellular, medium, and S-

layer fractions of bacteria for Western blot analysis. The results (Figure 6A) indicated that 100-kDa S-layer proteins were absent from VAR-F48 extracts but present in both WT and *spo0A*-complemented VAR-F48 samples. Figure 6B shows that synthesis of both Spo0A and the S-layer protein EA1 were restored in *spo0A*-complemented VAR-F48. Taken together, these results indicate that Spo0A regulates S-layer protein synthesis in *B. cereus*.

Discussion

The objective of this study was to determine the survival strategies used by *B. cereus* in groundwater. Like all other *Bacillus* species, *B. cereus* can form dormant endospores to resist adverse conditions. However, this survival strategy is energetically demanding and may only be used when the survival benefits offset the energy cost (Filippidou et al., 2016). Sporulation initiation has been extensively studied in *Bacillus subtilis:* the key event is the accumulation of the master response regulator Spo0A, under its activated phosphorylated form (Piggot and Hilbert, 2004). Phosphorylation of Spo0A is achieved by a multi-component phosphorelay, orthologs of which were found in species of the *B. cereus* group, indicating that sporulation initiation could occur in *B. cereus* by a process similar to that described in *B. subtilis*.

In this study, we showed that vegetative *B. cereus* F4810/72 forms endospore when inoculated in oligotrophic groundwater. Formation of endospore followed a period of rapid death that could have triggered sporulation (Liu et al., 2015). However, the endospore population did not persist, and was replaced by an asporogenic mutant population after long-term incubation. Accumulation of asporogenic mutants could result from endospore germination and accumulation of beneficial mutations. Non-persistent asporogenic mutants

have been described for several *Bacillus* species, including *B. thuringiensis* and *B. anthracis* (Sachidanandham and Jayaraman, 1993; Masel and Maughan, 2007; Maughan et al., 2007; Sastalla and Leppla, 2012). The data presented here show that such asporogenic mutants can accumulate in a natural medium exerting a strong survival pressure. *B. cereus* ATCC strain 14579 (Fig. S3) did not replicate this asporogenic evolution, indicating that this survival strategy is not common to all *B. cereus* strains. However, it should be noted that *B. cereus* F4810/72 and *B. cereus* ATCC 14579 are completely different genomospecies by literally any possible metric one could use to define "species" (Carroll et al., 2020). In addition, the *B. cereus*. ATCC 14579 type strain and the *B. cereus* emetic reference strain F4810/72 are classed in different phylogenetic groups (Groups IV and III, respectively (Guinebretiere et al., 2008)). This raises the question of the role of the *B. cereus* genetic background in the emergence of asporogenic mutant populations. This role will be determined by studying a representative number of group III *B. cereus* s.l. strains.

Genetic analysis of several asporogenic variants of *B. cereus* F4810/72 isolated from groundwater showed mutations of various types in the gene encoding the pleiotropic response regulator Spo0A. This observation suggested that *spo0A* mutations may be a direct response to the survival pressure imposed by groundwater in a germination context (Cairns et al., 1988). In VAR-F48, the *spo0A* mutation was accompanied by mutations in two other genes, which were absent from other variants. This result suggests that these genes are secondary targets of survival pressure, but that mutations may occasionally confer an additional fitness advantage.

Comparative proteomics analyses revealed that, unlike WT, VAR-F48 did not synthesize Spo0A, explaining why it fails to sporulate. In addition to not sporulating, VAR-F48

produced no cereulide biosynthesis proteins or S-layer proteins. Cereulide biosynthesis genes are known to be positively regulated by Spo0A (Ehling-Schulz et al., 2015). Our data also showed that Spo0A positively controls synthesis of the two S-layer proteins, EA1 and the Sap-like protein B7HXP4. These two proteins are synthesized at high levels in exponentially growing WT cells (5% of total Normalized Spectral Abundance Factor in our proteomics data), as reported for other bacteria (Sleytr et al., 2014). Lack of S-layer protein synthesis, S-layer assembly and maintenance at the cell surface constitutes a significant energy saving for VAR-F48, and other asporogenic cells (Sara and Sleytr, 2000). Beyond sporulation, cereulide and S-layer synthesis, in *B. cereus*, Spo0A probably regulates several other metabolic processes, like in *B. subtilis* including overflow metabolism (Tannler et al., 2008).

The results of the comparative proteomics analysis presented here suggest that the VAR-F48 genetic background sustains increased overflow metabolism, both in conditions of carbon excess (MOD_{50}) and in oligotrophic conditions. Overflow metabolism refers to a metabolic strategy that favors anaerobic fermentation/respiration pathways over aerobic respiration pathways, even in the presence of oxygen (Basan et al., 2015). Nitrate respiration and several fermentation pathways were up-regulated in growing VAR-F48 cells compared to WT, but only the lactate-producing pathway remained significantly up-regulated in starved cells from groundwater. Overflow metabolism is incompatible with efficient energy production, especially if lactate formation (which produces no ATP) is favored at the expense of aerobic respiration (Szenk et al., 2017). However, it allows rapid growth when carbon and energy are available, as observed for VAR-F48 in MOD_{50} medium. Rapid catabolism of carbon sources into organic acids is especially advantageous in a natural environment as a strategy to outcompete other

microorganisms (Silva et al., 2017). In oligotrophic conditions, such as those encountered in groundwater, energy management is a priority for survival, and we can propose various explanations for the maintenance of low energy-efficiency overflow metabolism in VAR-F48. One such explanation is that the biosynthetic cost of the fermentation pathway is lower than that for the electron transport chain (Basan et al., 2015). Alternatively, lack of initiation of sporulation allows VAR-F48 cells to save their remaining energy to adapt to long periods of starvation. Finally, overflow metabolism may be maintained due to carbon catabolite repression (CCR, (Dauner et al., 2001)).

In line with this last hypothesis, we found increased levels of the key regulator of CCR, CcpA, in groundwater cultures. In addition to regulating catabolic pathways, CcpA regulates the expression of virulence factors, especially toxins in *B. cereus* (van der Voort et al., 2008) and thus limits the energy expenditure required for their synthesis and secretion. Thus, in the absence of Spo0A, CcpA appeared to play an important role in proteome remodeling and orchestration of efficient energy use. Other general contributors to energy utilization and survival in groundwater may be the σB activating protein, Obg, and the DNA recombination/repair protein RecA proteins. The stringent response inhibits macromolecule synthesis (Dalebroux and Swanson, 2012) and may also play an important role in regulating glycolysis genes (Zhang et al., 2016). In summary, our results indicate that VAR-F48 lacks the Spo0A-dependent sporulation machinery needed to initiate sporulation, but its carefully regulated metabolic status allows it to remain viable in oligotrophic water.

VAR-F48 exhibits a typical GASP-like phenotype (Finkel, 2006), but how VAR-F48 cells find the energy resources needed to survive in groundwater remains open to question. Microscopic

observations revealed cell lysis in groundwater cultures, suggesting that nutrients to maintain *B. cereus* cells in an oligotrophic state could be obtained from dead cells.

In conclusion, in this work we showed that sporulation is not the only strategy used by *B. cereus* to survive in an oligotrophic environment. GASP-like mutants can emerge from *B. cereus* populations and survive in an asporogenic vegetative form. The advantage of vegetative forms over endospores is that vegetative cells can rapidly resume normal growth when nutrient conditions improve, whereas spore germination is time-consuming. Although it does not sporulate and its motility is impaired, VAR-F48 continues to produce biofilm. Biofilm formation could thus be important in contributing to its survival and persistence in a hostile environment.

Experimental procedures

Groundwater collection and sampling. Groundwater was collected from the superficial aquifer in an agricultural area near Avignon (France), as reported previously (Rousset et al., 2019). Samples were stored in acid-washed, autoclaved 20-L carbon-free polycarbonate Erlenmeyer flasks, and subsequently sterilized by autoclaving (120 °C for 20 min) before storage at – 20 °C. Calcite was removed from sterile groundwater by filtration at 0.22 µm (pore size). The physicochemical parameters of the groundwater were measured before and after treatment, and are shown in Table S5.

Bacterial strains and preculture. *Bacillus cereus* F4810/72 and its variants were stored at – 80 °C in 30% glycerol before use. Purity of the stock strains was verified (Shea et al., 2017).

Cryocultures were streaked onto LB medium and incubated for 72 h at 16 °C. A single colony was used to inoculate MOD_{50} medium, supplemented with 15 mM glucose (Rosenfeld et al., 2005), the initial OD_{600} was adjusted to 0.02, and the culture was incubated at 16 °C until the OD_{600} reached 0.07. Cells were then harvested by centrifugation at 10 000 x g, for 15 min at 16 °C. The pellet was washed twice with sterile groundwater, and subsequently used as inoculum.

Culture monitoring and isolation of variants. Aliquots of cultures were removed three times daily, serially diluted, spread onto LB agar plates, plates were supplemented with Congo Red where indicated, and incubated at 30 °C for 48 h (Worsham and Sowers, 1999). Plates with 50-150 colonies were examined carefully, and colonies that were translucent on LB agar and colorless on Congo Red-containing LB agar, were recorded as variants. Heat-resistant endospores were monitored by counting the cells resistant to a 15-min heat treatment at 70 °C. Percent of heat-resistant endospores, at one time point was determined as the ratio of the average number of heat-resistant CFUs to the average number of non-heated CFUs. A paired two-tailed t-test was used to determine significance of the difference ($p<0.05$) observed between heat-resistant endospore CFUs and non-heated CFU, using XLSTAT software. The Bonferroni method was used to calculate the adjusted *p*-values.

Results were log10 transformed (Log CFU/mL) and expressed as means ± standard deviation for each strain from three independent biological replicates. Survival kinetics were modeled for each strain using the biphasic model (Cerf, 1977). The biphasic model parameters (the fraction of the initial population in a major subpopulation (f), and the specific decay rates of the two

populations) were obtained using the Microsoft Excel® Add-in software, GInaFIT, available at KULeuven/BioTec3 and developed by Geeraerd et al. (2005).

Phenotypic assays. Oxidase activity was determined using oxidase reagent from Biomerieux (France). For sporulation assays, bacteria were grown in Fortified Nutrient Agar (FNA) sporulation medium for 48 h at 30 °C after inoculation (OD_{600nm}~ 0.002). Motility and biofilm assays were performed as previously described (Omer et al., 2015). All experiments were run in triplicate. We performed a repeated measures ANOVA test using the mixed models supplied by XLSTAT software to compare motility difference between WT and VAR-F48 strains. A two-tailed t-test was used to evaluate significance of difference observed between WT and VAR-F48 in biofilm assays, using XLSTAT software. The Bonferroni method was used to calculate the adjusted *p*-values.

Proteomics sample preparations. Groundwater medium (600 mL in 2-L carbon-free Erlenmeyer flask) was inoculated at an OD_{600} of 0.02. Bacteria were grown at 16 °C with continuous shaking (200 rpm) for approximately 72 h. Samples (200 mL) were collected after 0, 24 and 72 h incubation. Protein samples from cells and culture supernatants were prepared as previously described (Madeira et al., 2015; Madeira et al., 2016). Briefly, cells were homogenized in NuPAGE® LDS (Lithium dodecyl sulfate) sample buffer 1X (Thermofisher) supplemented with 5% β-mercaptoethanol. Homogenates were transferred to 2-ml vials containing silica beads. Samples were pre-treated by heating and ultrasound before producing

protein extracts by bead-beating in a Precellys Evolution instrument (Bertin Technologies) operated at 10,000 rpm for 10 cycles of 20 s, with 5 s rest between cycles.

Proteins from culture supernatants were TCA-precipitated, and the resulting pellets were dissolved in NuPAGE buffer.

Protein samples were treated as described elsewhere (Hartmann et al., 2014). Briefly, samples were loaded onto NuPAGE Bis-Tris 4–12% gels (Invitrogen) for a short 5-min migration at 200 V. Proteins were then digested in-gel with Mass Spectrometry Grade Trypsin Gold (Promega) in the presence of 0.01% ProteaseMAX surfactant (Promega). Triplicate samples were treated for both WT and VAR-F48 strains.

Protein identification by LC-MS/MS and label free quantification.

Peptide mixtures resulting from trypsin proteolysis were analyzed on a Q Exactive HF tandem mass spectrometer coupled to an UltiMate 3000 LC system (Dionex-LC Packings) in conditions similar to those previously described (Klein et al., 2016). Briefly, the peptide mixture was first desalted on-line on a reverse-phase precolumn (Acclaim PepMap 100 C18 column; 5 µm, 100 Å, 300 µm id, × 5 mm), and then resolved at a flow rate of 0.200 µL/min on a reverse-phase Acclaim PepMap 100 C18 column (3 µm, 100 Å, 75 µm id, × 500 mm). Solvent solutions were solvent A (0.1% formic acid) and solvent B (0.1% formic acid and 80% CH_3CN). For cellular proteins, a 90-min gradient (from 4% B to 25% in 75 min followed by an increase to 40% B) was applied; a 60-min gradient (from 2.5% B to 25% in 50 min followed by an increase to 40% B) was used for extracellular proteins. The instrument was operated in data-dependent

mode at a resolution of 60 000 to determine the masses of peptides, and applying a Top20 method with a dynamic exclusion of 10 s to select peptides for fragmentation.

MS/MS spectra were searched using the MASCOT Daemon software version 2.5.1 (Matrix Science) against the *B. cereus* AH187 NCBI_20180517 database. Parameters included trypsin digestion with a maximum of two missed cleavages, cysteine carbamidomethylation as fixed modification, methionine oxidation as variable modification, and mass tolerance of 5 ppm for peptides and 0.02 Da for MS/MS fragments. Peptide-to-Spectrum Matches were assigned when the *p*-value was below 0.05 in identity threshold mode. Proteins were validated when at least two distinct peptide sequences were assigned to them.

Proteomics data were deposited with the ProteomeXchange consortium (http://proteomecentral.proteomexchange.org) via the PRIDE (Perez-Riverol et al., 2019) partner repository (http://www.ebi.ac.uk/pride/), under dataset identifiers PXD018954 (cellular proteome) and PXD018955 (exoproteome).

Bioinformatics analyses. The DEP package for R (https://www.bioconductor.org/packages/release/bioc/html/DEP.html) was used to conduct PCA analysis and determine the significantly differentially accumulated proteins in VAR-F48 compared to WT (Zhang et al., 2018). The DEP package provided functions for data preparation, filtering, variance normalization and imputation of missing values, as well as statistical testing of differentially accumulated proteins (https://www.bioconductor.org/packages/release/bioc/manuals/DEP/man/DEP.pdf). We normalized data using variance stabilizing normalization (vsn). Analysis of protein differential

accumulation was based on protein-wise linear models and empirical Bayes statistics using limma. A protein was considered differentially accumulated as it exhibited a fold-change >1.5 and an adjusted *p*-value<0.05 with a false discovery rate <5%.

Protein functions were assigned using the Clusters of Orthologous Groups (COG) database (Galperin et al., 2015).

The Venn diagram was produced using Venny 2.1.0 software (https://bioinfogp.cnb.csic.es/tools/venny/).

Genomic re-sequencing and PCR analyses. This work has benefited from the facilities and expertise of the high throughput sequencing core facility of I2BC (Centre de Recherche de Gif – http://www.i2bc.paris-saclay.fr/). Genomic DNA of *B. cereus* F4810 (AH187) WT and F48-VAR were isolated using a Genomic DNA isolation kit (Qiagen). Genomic DNA libraries were prepared according to the Nextera DNA library preparation kit (Illumina) protocols. The pooled DNA from each experiment was then subjected to sequencing on an Illumina NextSeq instrument, using a NextSeq 500/550 high output kit v2 (75 cycles, (Illumina) and 75 nucleotide reads. Polymorphisms (SNPs and INDELs) were identified by comparing the *B. cereus* AH187 (F4810/72) reference genome (GCA_000021225.1), *B. cereus* F4810/72 WT lab strain and VAR-F48 mutant (Naquin et al., 2014). The data analysis pipeline included bcl2fastq2-2.18.12 (demultiplex, https://emea.support.illumina.com), Cutadapt 1.15 (adapter trimming, https://cutadapt.readthedocs.io/en/v1.15/guide.html), FastQC v0.11.5 (quality control, https://www.bioinformatics.babraham.ac.uk/projects/fastqc/), BWA 0.6.2-r126 (mapping, (Li and Durbin, 2010)), samtools 1.3 (coverage profile, (Li et al., 2009)), VarScan v2.3.9 (variant

detection, (Koboldt et al., 2012)) and snpEff 4_1b (mutation, (Cingolani et al., 2012)) with default parameters. Sequencing data were deposited in NCBI Biosample data base, via SRA Submission Portal Wizard, under dataset identifiers SAMN15808881, SAMN15808882.

Genomic analysis identified mutations in *spo0A*, *ctaA* and BCAH187_A2382, which were confirmed by re-sequencing PCR products.

The sequences of primers used for PCR analysis in this study are listed in Table S6.

Complementation. To complement the *spo0A* mutation in trans, the 1485-bp locus was first amplified using primer pairs X and Y (Table S6), it was then cloned into pCR-TOPO 2.1. The PCR fragment was cut with BamHI and SacI and ligated to a similarly digested pHT304 vector (Arantes and Lereclus, 1991). For *ctaA* complementation, the 1477-bp locus was amplified using the primers up-ctaA and down-ctaA (Table S6) and cloned into pCR-TOPO 2.1. The insert was cut with HindIII and SacI and ligated into the pHT304 vector digested with the same enzymes. The integrity of the genes in the recombinant vectors were verified by sequencing.

All recombinant vectors were introduced into *B. cereus* VAR-F48 by electroporation.

Mutant construction. Deletion of BCAH187_A2382 was achieved by allelic replacement, using the temperature-sensitive pMAD (Arnaud et al., 2004). Briefly, 1-kbp flanking DNA sequences upstream and downstream of the BCAH187_A2382 gene were amplified using the appropriate oligonucleotide primers (Table S6). The recombinant PCR products containing DNA sequences upstream and downstream of the BCAH187_A2382 gene were cloned into pCR-TOPO 2.1. The resulting plasmid was digested with *SmaI* and ligated with a *SmaI*-digested

spectinomycin fragment. The *EcoRI* fragment from the resulting plasmids was cloned into pMAD digested by the same enzyme. The recombinant plasmid was used to transform *B. cereus* F4810/72. The BCAH187_A2382 gene was deleted by a double-crossover event, as previously described (Arnaud et al., 2004). Chromosomal allele exchange was confirmed by PCR with oligonucleotide primers located upstream and downstream of the DNA regions used for allelic exchange.

Cell fractionation and Western blot analysis. Overnight cultures were diluted in LB medium to an OD_{600} of 0.03 and incubated at 30 °C until the OD_{600} reached 1. Cultures were centrifuged for 5 min at 8 000 × g and separated into medium (supernatant) and pellet fractions. Proteins in the medium were precipitated with 10% (vol/vol) trichloroacetic acid (TCA) for 30 min on ice and centrifuged at 16 000 × *g* for 10 min. Bacterial sediments (pellets) were washed twice with PBS and boiled (100 °C) for 10 min in 160 µL PBS–3 M urea to extract S-layer and S-layer-associated proteins. Extracts were centrifuged at 16 000 × *g*, and the S-layer extract was isolated from the bacterial sediment. The S-layer extract was added to an equal volume of sample buffer (4% SDS, 1% β-mercaptoethanol, 10% glycerol, 50 mM Tris-HCl [pH 7.5], 0.01% bromophenol blue). The bacterial sediment was washed twice with PBS before mechanical lysis by silica bead-beating for 5 min (FastPrep-24; MP Biomedical). The beads were sedimented to isolate cell lysates. Proteins in the cell lysates were TCA-precipitated and collected by centrifugation at 16 000 × *g* for 10 min. All TCA precipitates were washed with ice-cold acetone and dried. Samples were suspended in 160 µL 1-M Tris-HCl (pH 8.0)–4% SDS and mixed with an equal volume of sample buffer. Aliquots (15 µL) of each sample were separated

on 10% SDS-PAGE gels and analyzed by Coomassie staining or after transfer to nitrocellulose membranes for immunoblot analysis. Proteins were detected using rabbit antiserum raised against purified EA1 and Spo0A, gifts from Dominique Missiakas (University of Chicago) and Masaya Fujita (University of Houston), respectively. Immunoreactive products were revealed by chemiluminescent detection after incubation with horseradish peroxidase (HRP)-conjugated anti-rabbit antibody.

Acknowledgments

The authors thank Avignon University foundation for providing financial support for LR's PhD.

Table and Figure legends

Figure 1. Survival response of *B. cereus* F4810/72 (WT) in groundwater over a 30-day incubation period at 16 °C. **Panel A**: CFU counts on LB agar plates. Green trace, total count; black trace, heat-resistant colonies; red trace, colonies with variant morphology. Each value corresponds to the mean of three independent biological replicates ± SD. The difference between total and heat-resistant count was significant before the first two days and after day 5 (Bonferroni adjusted p value<0.05, paired two tailed t-test). The difference between total and variant counts becomes not significant after day 5. **Panel B**: Colony morphology of WT and variants on LB agar. **Panel C**: Colony morphology of WT and variants on Congo Red-supplemented LB agar. Arrows indicate morphological variants.

Figure 2. Survival curves of *B. cereus* VAR-F48 and WT in groundwater over 30 days' incubation at 16 °C. Log(CFU) for WT are indicated with squares, and Log(CFU) for VAR-F48 are indicated with circles. The three biological replicates are shown for each strain. The red and blue curves represent theoretical data obtained with the biphasic model. The specific rates of decays are 0.54±0.2 day^{-1} and 0.14±0.06 day^{-1} in the first (day 0 to day 3), and the second phase (after day 3), respectively for VAR-F48. The specific rates of decays are 1.47±0.65 day^{-1} and 0.04±0.02 day^{-1} in the first (day 0 to day 13), and the second phase (after day 13), respectively for WT. These values are significantly different in VAR-F48 compared to WT (Bonferroni adjusted *p* value $p<0.05$ according to unpaired t-test).

Figure 3. Dynamics of differentially accumulated proteins (DAPs) between VAR-F48 and its parental strain (WT). **Panel A**: **Total protein fraction**. PCA was performed to compare the distribution of the three biological replicates at each time-point for both WT and VAR-F48. The axis labels indicate percentage of total variance, which is explained by the first (PC1) and second component (PC2). **Panel B**: **DAPs**. Venn diagram shows the number of DAPs at each time-point and the overlaps between time-points. The Venn diagram was drawn with Venny. T0, T1 and T2 correspond to 0, 24 and 72-h incubation time in groundwater.

Figure 4. Clusters of Orthologous Groups (COG) distribution of exclusive DAPs. DAPs were clustered at T0, T1 (24 h) and T2 (72 h). Number of enhanced-DAPs are indicated in red and decreased-DAPs in blue, in each COG group.

Figure 5. Biofilm development and motility of VAR-F48 and WT *B. cereus* strains. **Panel A**. Biofilm formation by VAR-F48 (red) and WT (blue). Biofilm formation was assessed by measuring OD_{595nm}. Data correspond to the mean ± SD of ten assays. Significant differences are indicated by asterisks (Bonferroni adjusted *p* value $p<0.05$ in unpaired two-tailed t-test). **Panel B**. Swimming motility of VAR-F48 (blue) and WT (red). Diameters of motility haloes were measured on TrB plates containing 0.25% agar. **Panel C**. Swarming motility of VAR-F48 (blue) and WT (red). Diameters of motility haloes were measured on TrB plates containing 0.7% agar. Data correspond to the mean ± SD of triplicate assays.

Figure 6. SDS-PAGE and Western-blot analysis of VAR-F48 and WT protein extracts. **Panel A.** Coomassie stained SDS PAGE gel. Total protein extracts from the cellular fraction (C), medium fraction (M) and S-layer fraction (S) were separated on 10% SDS PAGE and stained with Coomassie blue. **Panel B**. EA1 and Spo0A immuno-detection. Proteins separated on SDS-PAGE were transferred onto nitrocellulose membranes for immunoblotting with polyclonal anti-Spo0A and anti-EA1 serum. Protein extracts were prepared from LB cultures of WT, VAR-F48 and VAR-F48 transformed with the complementing plasmid pHT304-*spo0A*.

Table 1. Cellular proteins for which differential accumulation was measured between WT and VAR-F48 after 0 h, 24 h and 48 h incubation in groundwater.

Table 2. Cellular proteins for which differential accumulation was measured between WT and VAR-F48 after both 24 h and 72 h incubation in groundwater.

Table 3: Exoproteins for which differential accumulation was measured in VAR-F48 compared to WT after 24 h and/or 72 h incubation in groundwater.

Supplementary data

Figure S1. DNA sequences and translation of genes identified as mutated in VAR-F48 and other variants isolated from groundwater.

Figure S2. Cultures of *B. cereus* strains in groundwater medium at 16 °C for proteomics analysis. Panel A: CFU counts for WT colonies, total (blue) and heat-resistant colonies (black). Panel B: CFU counts for VAR-F48 (red). Each value corresponds to the mean of three independent biological replicates ± SD. T0, T1, and T2 correspond to the sampling times used for the proteomics analysis.

Figure S3. Survival response of *B. cereus* ATCC 14579 in groundwater over 70 days at 16 °C. Red, total colony count; black, heat-resistant colony count. Values correspond to the mean from three independent biological replicates ± SD.

Table S1: Proteins identified in the cellular proteomes of F4810/72 (WT) and VAR-F48 strains.

Table S2: Cellular proteins showing differential accumulation between WT and VAR-F48.

Table S3: Proteins identified in exoproteomes from F4810/72 (WT) and VAR-F48 strains.

Table S4: Extracellular proteins showing differential accumulation between WT and VAR-F48.

Table S5: Physicochemical characteristics of groundwater used to cultivate *B. cereus*.

Table S6: Primers used in this study.

References

Agata, N., Ohta, M., and Yokoyama, K. (2002) Production of *Bacillus cereus* emetic toxin (cereulide) in various foods. *Int J Food Microbiol* **73**: 23-27.

Arantes, O., and Lereclus, D. (1991) Construction of cloning vectors for *Bacillus thuringiensis*. *Gene* **108**: 115-119.

Arnaud, M., Chastanet, A., and Debarbouille, M. (2004) New vector for efficient allelic replacement in naturally nontransformable, low-GC-content, gram-positive bacteria. *Appl Environ Microbiol* **70**: 6887-6891.

Basan, M., Hui, S., Okano, H., Zhang, Z., Shen, Y., Williamson, J.R., and Hwa, T. (2015) Overflow metabolism in *Escherichia coli* results from efficient proteome allocation. *Nature* **528**: 99-104.

Bendtsen, J.D., Kiemer, L., Fausboll, A., and Brunak, S. (2005) Non-classical protein secretion in bacteria. *BMC Microbiol* **5**: 58.

Brillard, J., Dupont, C.M., Berge, O., Dargaignaratz, C., Oriol-Gagnier, S., Doussan, C. et al. (2015) The Water Cycle, a Potential Source of the Bacterial Pathogen *Bacillus cereus*. *Biomed Res Int* **2015**: 356928.

Cairns, J., Overbaugh, J., and Miller, S. (1988) The origin of mutants. *Nature* **335**: 142-145.

Carlin, F., Brillard, J., Broussolle, V., Clavel, T., Duport, C., Jobin, M. et al. (2010) Adaptation of Bacillus cereus, an ubiquitous worldwide-distributed foodborne pathogen, to a changing environment. *Food Research International* **43**: 1885-1894.

Carroll, L.M., Wiedmann, M., and Kovac, J. (2020) Proposal of a Taxonomic Nomenclature for the *Bacillus cereus* Group Which Reconciles Genomic Definitions of Bacterial Species with Clinical and Industrial Phenotypes. *mBio* **11**.

Carroll, L.M., Wiedmann, M., Mukherjee, M., Nicholas, D.C., Mingle, L.A., Dumas, N.B. et al. (2019) Characterization of Emetic and Diarrheal *Bacillus cereus* Strains From a 2016 Foodborne Outbreak Using Whole-Genome Sequencing: Addressing the Microbiological, Epidemiological, and Bioinformatic Challenges. *Front Microbiol* **10**: 144.

Cerf, O. (1977) Tailing of survival curves of bacterial spores. *J Appl Bacteriol* **42**: 1-19.

Cingolani, P., Platts, A., Wang le, L., Coon, M., Nguyen, T., Wang, L. et al. (2012) A program for annotating and predicting the effects of single nucleotide polymorphisms, SnpEff: SNPs in the genome of Drosophila melanogaster strain w1118; iso-2; iso-3. *Fly (Austin)* **6**: 80-92.

Clair, G., Lorphelin, A., Armengaud, J., and Duport, C. (2013) OhrRA functions as a redox-responsive system controlling toxinogenesis in Bacillus cereus. *J Proteomics* **94**: 527-539.

Classen, A.T., Sundqvist, M.K., Henning, J.A., Newman, G.S., Moore, J.A.M., Cregger, M.A. et al. (2015) Direct and indirect effects of climate change on soil microbial and soil microbial-plant interactions: What lies ahead? *Ecosphere* **6**: 1-21.

Dalebroux, Z.D., and Swanson, M.S. (2012) ppGpp: magic beyond RNA polymerase. *Nat Rev Microbiol* **10**: 203-212.

Dauner, M., Storni, T., and Sauer, U. (2001) *Bacillus subtilis* metabolism and energetics in carbon-limited and excess-carbon chemostat culture. *J Bacteriol* **183**: 7308-7317.

Dillon, P., Page, D., Vanderzalm, J., Pavelic, P., Toze, S., Bekele, E. et al. (2008) A critical evaluation of combined engineered and aquifer treatment systems in water recycling. *Water Sci Technol* **57**: 753-762.

Drobniewski, F.A. (1993) *Bacillus cereus* and related species. *Clin Microbiol Rev* **6**: 324-338.

Duport, C., Jobin, M., and Schmitt, P. (2016) Adaptation in *Bacillus cereus*: From Stress to Disease. *Front Microbiol* **7**: 1550.

Duport, C., Zigha, A., Rosenfeld, E., and Schmitt, P. (2006) Control of enterotoxin gene expression in Bacillus cereus F4430/73 involves the redox-sensitive ResDE signal transduction system. *J Bacteriol* **188**: 6640-6651.

Ehling-Schulz, M., Frenzel, E., and Gohar, M. (2015) Food-bacteria interplay: pathometabolism of emetic *Bacillus cereus*. *Front Microbiol* **6**: 704.

Ehling-Schulz, M., Lereclus, D., and Koehler, T.M. (2019) The *Bacillus cereus* Group: Bacillus Species with Pathogenic Potential. *Microbiol Spectr* **7**.

Filippidou, S., Wunderlin, T., Junier, T., Jeanneret, N., Dorador, C., Molina, V. et al. (2016) A Combination of Extreme Environmental Conditions Favor the Prevalence of Endospore-Forming Firmicutes. *Front Microbiol* **7**: 1707.

Fimlaid, K.A., and Shen, A. (2015) Diverse mechanisms regulate sporulation sigma factor activity in the Firmicutes. *Curr Opin Microbiol* **24**: 88-95.

Finkel, S.E. (2006) Long-term survival during stationary phase: evolution and the GASP phenotype. *Nat Rev Microbiol* **4**: 113-120.

Galperin, M.Y., Makarova, K.S., Wolf, Y.I., and Koonin, E.V. (2015) Expanded microbial genome coverage and improved protein family annotation in the COG database. *Nucleic Acids Res* **43**: D261-269.

Garcia Costas, A.M., Poudel, S., Miller, A.F., Schut, G.J., Ledbetter, R.N., Fixen, K.R. et al. (2017) Defining Electron Bifurcation in the Electron-Transferring Flavoprotein Family. *J Bacteriol* **199**.

Geeraerd, A.H., Valdramidis, V.P., and Van Impe, J.F. (2005) GInaFiT, a freeware tool to assess non-log-linear microbial survivor curves. *Int J Food Microbiol* **102**: 95-105.

Gigliobianco, T., Lakaye, B., Wins, P., El Moualij, B., Zorzi, W., and Bettendorff, L. (2010) Adenosine thiamine triphosphate accumulates in *Escherichia coli* cells in response to specific conditions of metabolic stress. *BMC Microbiol* **10**: 148.

Gonzalez, I., Lopez, M., Mazas, M., Gonzalez, J., and Bernardo, A. (1995) The effect of recovery conditions on the apparent heat resistance of *Bacillus cereus* spores. *J Appl Bacteriol* **78**: 548-554.

Gorke, B., and Stulke, J. (2008) Carbon catabolite repression in bacteria: many ways to make the most out of nutrients. *Nat Rev Microbiol* **6**: 613-624.

Green, T.R., and Anapalli, S.S. (2018) Irrigation variability and climate change affect derived distributions of simulated water recharge and nitrate leaching. *Water International* **43**: 829-845.

Guinebretiere, M.H., Velge, P., Couvert, O., Carlin, F., Debuyser, M.L., and Nguyen-The, C. (2010) Ability of *Bacillus cereus* group strains to cause food poisoning varies according to phylogenetic affiliation (groups I to VII) rather than species affiliation. *J Clin Microbiol* **48**: 3388-3391.

Guinebretiere, M.H., Thompson, F.L., Sorokin, A., Normand, P., Dawyndt, P., Ehling-Schulz, M. et al. (2008) Ecological diversification in the *Bacillus cereus* Group. *Environ Microbiol* **10**: 851-865.

Guinebretiere, M.H., Auger, S., Galleron, N., Contzen, M., De Sarrau, B., De Buyser, M.L. et al. (2013) *Bacillus cytotoxicus* sp. nov. is a novel thermotolerant species of the *Bacillus cereus* Group occasionally associated with food poisoning. *Int J Syst Evol Microbiol* **63**: 31-40.

Hartmann, E.M., Allain, F., Gaillard, J.C., Pible, O., and Armengaud, J. (2014) Taking the shortcut for high-throughput shotgun proteomic analysis of bacteria. *Methods Mol Biol* **1197**: 275-285.
Holden, J.K., Li, H., Jing, Q., Kang, S., Richo, J., Silverman, R.B., and Poulos, T.L. (2013) Structural and biological studies on bacterial nitric oxide synthase inhibitors. *Proc Natl Acad Sci U S A* **110**: 18127-18131.
Jessberger, N., Krey, V.M., Rademacher, C., Bohm, M.E., Mohr, A.K., Ehling-Schulz, M. et al. (2015) From genome to toxicity: a combinatory approach highlights the complexity of enterotoxin production in *Bacillus cereus*. *Front Microbiol* **6**: 560.
John, D.E., and Rose, J.B. (2005) Review of factors affecting microbial survival in groundwater. *Environ Sci Technol* **39**: 7345-7356.
Kern, V.J., Kern, J.W., Theriot, J.A., Schneewind, O., and Missiakas, D. (2012) Surface-layer (S-layer) proteins sap and EA1 govern the binding of the S-layer-associated protein BslO at the cell septa of *Bacillus anthracis*. *J Bacteriol* **194**: 3833-3840.
Kint, C., Verstraeten, N., Hofkens, J., Fauvart, M., and Michiels, J. (2014) Bacterial Obg proteins: GTPases at the nexus of protein and DNA synthesis. *Crit Rev Microbiol* **40**: 207-224.
Klein, G., Mathe, C., Biola-Clier, M., Devineau, S., Drouineau, E., Hatem, E. et al. (2016) RNA-binding proteins are a major target of silica nanoparticles in cell extracts. *Nanotoxicology* **10**: 1555-1564.
Ko, M., Choi, H., and Park, C. (2002) Group I self-splicing intron in the recA gene of *Bacillus anthracis*. *J Bacteriol* **184**: 3917-3922.
Koboldt, D.C., Zhang, Q., Larson, D.E., Shen, D., McLellan, M.D., Lin, L. et al. (2012) VarScan 2: somatic mutation and copy number alteration discovery in cancer by exome sequencing. *Genome Res* **22**: 568-576.
Kolsto, A.B., Tourasse, N.J., and Okstad, O.A. (2009) What sets *Bacillus anthracis* apart from other *Bacillus* species? *Annu Rev Microbiol* **63**: 451-476.
Lebeuf-Taylor, E., McCloskey, N., Bailey, S.F., Hinz, A., and Kassen, R. (2019) The distribution of fitness effects among synonymous mutations in a gene under directional selection. *Elife* **8**.
Lever, M.A., Rogers, K.L., Lloyd, K.G., Overmann, J., Schink, B., Thauer, R.K. et al. (2015) Life under extreme energy limitation: a synthesis of laboratory- and field-based investigations. *FEMS Microbiol Rev* **39**: 688-728.
Li, H., and Durbin, R. (2010) Fast and accurate long-read alignment with Burrows-Wheeler transform. *Bioinformatics* **26**: 589-595.
Li, H., Handsaker, B., Wysoker, A., Fennell, T., Ruan, J., Homer, N. et al. (2009) The Sequence Alignment/Map format and SAMtools. *Bioinformatics* **25**: 2078-2079.
Liu, Y., Lai, Q., Du, J., and Shao, Z. (2017) Genetic diversity and population structure of the *Bacillus cereu*s group bacteria from diverse marine environments. *Sci Rep* **7**: 689.
Liu, Z., Qiao, K., Tian, L., Zhang, Q., Liu, Z.Y., and Li, F.L. (2015) Spontaneous large-scale autolysis in *Clostridium acetobutylicum* contributes to generation of more spores. *Front Microbiol* **6**: 950.
Lucking, G., Frenzel, E., Rutschle, A., Marxen, S., Stark, T.D., Hofmann, T. et al. (2015) Ces locus embedded proteins control the non-ribosomal synthesis of the cereulide toxin in emetic *Bacillus cereus* on multiple levels. *Front Microbiol* **6**: 1101.
Madeira, J.P., Alpha-Bazin, B., Armengaud, J., and Duport, C. (2015) Time dynamics of the Bacillus cereus exoproteome are shaped by cellular oxidation. *Front Microbiol* **6**: 342.
Madeira, J.P., Omer, H., Alpha-Bazin, B., Armengaud, J., and Duport, C. (2016) Deciphering the interactions between the Bacillus cereus linear plasmid, pBClin15, and its host by high-throughput comparative proteomics. *J Proteomics* **146**: 25-33.

Masel, J., and Maughan, H. (2007) Mutations leading to loss of sporulation ability in *Bacillus subtilis* are sufficiently frequent to favor genetic canalization. *Genetics* **175**: 453-457.
Maughan, H., Masel, J., Birky, C.W., Jr., and Nicholson, W.L. (2007) The roles of mutation accumulation and selection in loss of sporulation in experimental populations of *Bacillus subtilis*. *Genetics* **177**: 937-948.
Moore, C.M., Nakano, M.M., Wang, T., Ye, R.W., and Helmann, J.D. (2004) Response of *Bacillus subtilis* to nitric oxide and the nitrosating agent sodium nitroprusside. *J Bacteriol* **186**: 4655-4664.
Mueller, J.P., and Taber, H.W. (1989) Isolation and sequence of ctaA, a gene required for cytochrome aa3 biosynthesis and sporulation in *Bacillus subtilis*. *J Bacteriol* **171**: 4967-4978.
Naquin, D., d'Aubenton-Carafa, Y., Thermes, C., and Silvain, M. (2014) CIRCUS: a package for Circos display of structural genome variations from paired-end and mate-pair sequencing data. *BMC Bioinformatics* **15**: 198.
Omer, H., Alpha-Bazin, B., Brunet, J.L., Armengaud, J., and Duport, C. (2015) Proteomics identifies *Bacillus cereus* EntD as a pivotal protein for the production of numerous virulence factors. *Front Microbiol* **6**: 1004.
Perez-Riverol, Y., Csordas, A., Bai, J., Bernal-Llinares, M., Hewapathirana, S., Kundu, D.J. et al. (2019) The PRIDE database and related tools and resources in 2019: improving support for quantification data. *Nucleic Acids Res* **47**: D442-D450.
Pfrunder, S., Grossmann, J., Hunziker, P., Brunisholz, R., Gekenidis, M.T., and Drissner, D. (2016) *Bacillus cereus* Group-Type Strain-Specific Diagnostic Peptides. *J Proteome Res* **15**: 3098-3107.
Piggot, P.J., and Hilbert, D.W. (2004) Sporulation of *Bacillus subtilis*. *Curr Opin Microbiol* **7**: 579-586.
Plaut, R.D., Beaber, J.W., Zemansky, J., Kaur, A.P., George, M., Biswas, B. et al. (2014) Genetic evidence for the involvement of the S-layer protein gene sap and the sporulation genes *spo0A*, *spo0B*, and *spo0F* in Phage AP50c infection of *Bacillus anthracis*. *J Bacteriol* **196**: 1143-1154.
Pulschen, A.A., Sastre, D.E., Machinandiarena, F., Crotta Asis, A., Albanesi, D., de Mendoza, D., and Gueiros-Filho, F.J. (2017) The stringent response plays a key role in *Bacillus subtilis* survival of fatty acid starvation. *Mol Microbiol* **103**: 698-712.
Ramarao, N., and Sanchis, V. (2013) The pore-forming haemolysins of *Bacillus cereus*: a review. *Toxins (Basel)* **5**: 1119-1139.
Rosenfeld, E., Duport, C., Zigha, A., and Schmitt, P. (2005) Characterization of aerobic and anaerobic vegetative growth of the food-borne pathogen Bacillus cereus F4430/73 strain. *Can J Microbiol* **51**: 149-158.
Rousset, L., Gillon, M., Duport, C., Clavel, C., Lagree, M., Traika, M. et al. (2019) A first inventory of the labile biochemicals found in Avignon groundwater: can we identify potential bacterial substrates? In *i-DUST 2018 – Inter-Disciplinary Underground Science & Technology* EDP Sciences.
Sachidanandham, R., and Jayaraman, K. (1993) Formation of spontaneous asporogenic variants of *Bacillus thuringiensis* subsp. galleriaein continuous cultures. *Appl Microbiol Biotechnol* **40**: 504-507.
Saleem, S., Levison, J., Parker, B., Martin, R., and Persaud, E. (2020) Impacts of Climate Change and Different Crop Rotation Scenarios on Groundwater Nitrate Concentrations in a Sandy Aquifer *sustainability* **12**: 1153.
Salvetti, S., Ghelardi, E., Celandroni, F., Ceragioli, M., Giannessi, F., and Senesi, S. (2007) FlhF, a signal recognition particle-like GTPase, is involved in the regulation of flagellar arrangement, motility behaviour and protein secretion in *Bacillus cereus*. *Microbiology* **153**: 2541-2552.
Sara, M., and Sleytr, U.B. (2000) S-Layer proteins. *J Bacteriol* **182**: 859-868.

Sastalla, I., and Leppla, S.H. (2012) Occurrence, recognition, and reversion of spontaneous, sporulation-deficient *Bacillus anthracis* mutants that arise during laboratory culture. *Microbes Infect* **14**: 387-391.

Scott, J.M., and Haldenwang, W.G. (1999) Obg, an essential GTP binding protein of *Bacillus subtilis,* is necessary for stress activation of transcription factor sigma(B). *J Bacteriol* **181**: 4653-4660.

Shea, A.A., Bernhards, R.C., Cote, C.K., Chase, C.J., Koehler, J.W., Klimko, C.P. et al. (2017) Two stable variants of *Burkholderia pseudomallei* strain MSHR5848 express broadly divergent in vitro phenotypes associated with their virulence differences. *PLoS One* **12**: e0171363.

Shu, J.C., Soo, P.C., Chen, J.C., Hsu, S.H., Chen, L.C., Chen, C.Y. et al. (2013) Differential regulation and activity against oxidative stress of Dps proteins in *Bacillus cereus*. *Int J Med Microbiol* **303**: 662-673.

Siebert, S., Burke, J., Faures, J.M., Frenken, K., Hoogeveen, J., Doll, P., and Portmann, F.T. (2010) Groundwater use for irrigation - a global inventory. *Hydrology and Earth System Sciences* **14**: 1863-1880.

Silva, I.N., Ramires, M.J., Azevedo, L.A., Guerreiro, A.R., Tavares, A.C., Becker, J.D., and Moreira, L.M. (2017) Regulator LdhR and d-Lactate Dehydrogenase LdhA of *Burkholderia multivorans* Play Roles in Carbon Overflow and in Planktonic Cellular Aggregate Formation. *Appl Environ Microbiol* **83**.

Sleytr, U.B., Schuster, B., Egelseer, E.M., and Pum, D. (2014) S-layers: principles and applications. *FEMS Microbiol Rev* **38**: 823-864.

Stenfors Arnesen, L.P., Fagerlund, A., and Granum, P.E. (2008) From soil to gut: *Bacillus cereus* and its food poisoning toxins. *FEMS Microbiol Rev* **32**: 579-606.

Szenk, M., Dill, K.A., and de Graff, A.M.R. (2017) Why Do Fast-Growing Bacteria Enter Overflow Metabolism? Testing the Membrane Real Estate Hypothesis. *Cell Syst* **5**: 95-104.

Tannler, S., Decasper, S., and Sauer, U. (2008) Maintenance metabolism and carbon fluxes in *Bacillus* species. *Microb Cell Fact* **7**: 19.

van der Voort, M., Kuipers, O.P., Buist, G., de Vos, W.M., and Abee, T. (2008) Assessment of CcpA-mediated catabolite control of gene expression in *Bacillus cereus* ATCC 14579. *BMC Microbiol* **8**: 62.

Worsham, P.L., and Sowers, M.R. (1999) Isolation of an asporogenic (spoOA) protective antigen-producing strain of *Bacillus anthracis*. *Can J Microbiol* **45**: 1-8.

Zhang, T., Zhu, J., Wei, S., Luo, Q., Li, L., Li, S. et al. (2016) The roles of RelA/(p)ppGpp in glucose-starvation induced adaptive response in the zoonotic *Streptococcus suis*. *Sci Rep* **6**: 27169.

Zhang, X., Smits, A.H., van Tilburg, G.B., Ovaa, H., Huber, W., and Vermeulen, M. (2018) Proteome-wide identification of ubiquitin interactions using UbIA-MS. *Nat Protoc* **13**: 530-550.

Zhou, Y., Zwahlen, F., Wang, Y., and Li, Y. (2010) Impact of climate change on irrigation requirements in terms of groundwater resources. *Hydrogeology Journal* **18**: 1571-1582.

Table 1. Cellular proteins for which differential accumulation was measured between WT and VAR-F48 after 0 h, 24 h and 48 h incubation in groundwater.

	ORF	Gene	Description	$Log_2(FC)^1$		
				0	24h	72h
Decreased in VAR-F48						
Cell wall/membrane/envelope biogenesis						
B7HXP5	BCAH187_A1065	eag	S-layer protein EA1	-7.68	-7.98	-7.4
B7HXP4	BCAH187_A1064		Crystal protein	-3.07	-3.02	-3.38
B7HYF0	BCAH187_A5568		Putative D-alanyl-D-alanine carboxypeptidase	-1.2	-2.54	-2
B7HNA1	BCAH187_A2059		Putative cell wall peptidase	-1.13	-1.64	-4.01
Defense mechanisms						
B7HPH5	BCAH187_A4408	sodA1	Superoxide dismutase (EC 1.15.1.1)	-2.06	-1.74	-1.77
B7HKH2	BCAH187_A1610	hmp	Flavohemoprotein	1.56	2.44	3.45
Unknown function						
B7HU83	BCAH187_A0625		AAA_PrkA domain-containing protein	-2.51	-4.47	-5.65
Pathogenesis						
Q20CI6		cesD	Putative permease	-2.14	-2.86	-2.56
A1BYG6		cesC	ABC transporter ATP-binding protein	-2.01	-2.72	-2.81
Transcription						
B7HNT4	BCAH187_A4301	spo0A	Stage 0 sporulation protein A	-4.61	-3.82	-4.02
Transport						
B7HWE1	BCAH187_A0847		Transporter AcrB/AcrD/AcrF family	-3.78	-3.34	-3.45
Enhanced in VAR-F48						
Carbohydrate transport and metabolism						
B7HTY2	BCAH187_A5012	ldh	L-lactate dehydrogenase (L-LDH)	1.81	3.64	5.12
Coenzyme transport and metabolism						
B7HWF3	BCAH187_A0885	thiS	Thiamine biosynthesis protein ThiS	1.83	3.61	3.85
General function prediction only						
B7HT11	BCAH187_A0426		Putative linear gramicidin synthetase subunit B	1.8	3.36	3.39

[1] FC: fold-change. *i.e*. NSAF ratio VAR-F48 vs WT

Table 2. Cellular proteins for which differential accumulation was measured between WT and VAR-F48 after both 24 h and 72 h incubation in groundwater.

Uniprot-ID	Gene	ORF	Description	$Log_2(FC)$[1] 24h	$Log_2(FC)$[1] 72h
Decreased in VAR-F48					
Lipid transport and metabolism					
B7IOM3	phaC	BCAH187_A1471	Poly(R)-hydroxyalkanoic acid synthase	-1.92	-2.08
Sporulation					
B7HLA4	cotE	BCAH187_A3817	Spore coat protein E	-4.75	-7.19
Transcription					
B7HM25	sigE	BCAH187_A3957	RNA polymerase sigma factor	-4.24	-4
Up-DAPs					
Amino acid transport and metabolism					
B7HVI1	hisC	BCAH187_A3002	Histidinol-phosphate aminotransferase	2.6	2.83
B7I0E7	trpE	BCAH187_A1393	Anthranilate synthase component 1	2.97	4.2
B7I0F0	trpC	BCAH187_A1396	Indole-3-glycerol phosphate synthase	3.1	2.68
Cell wall/membrane/envelope biogenesis					
B7HPF3	murG	BCAH187_A4384	UDP-N-acetylglucosamine	3.09	3.72
B7HZM0		BCAH187_A1252	Putative S-layer protein	3.25	4.29
Coenzyme transport and metabolism					
B7HWF4	thiG	BCAH187_A0886	Thiazole synthase	1.95	2.78
B7HT70	thiE	BCAH187_A0487	Thiamine-phosphate synthase	2.66	3.5
Unknown function					
B7HK89		BCAH187_A1524	Putative Fumaryl acetoacetate hydrolase	3.05	3.37
B7HYD6		BCAH187_A5554	YwhD family protein	3.11	3.33
General function predicted					
B7HV44		BCAH187_A0666	Putative prophage LambdaBa01	1.76	1.87
Signal transduction mechanisms					
B7HQ84		BCAH187_A2400	Sensor histidine kinase	3.36	3.26
Transcription					
B7HSL3	ccpA	BCAH187_A4811	Catabolite control protein A	1.23	1.71
Translation. ribosomal structure and biogenesis					
B7HU81		BCAH187_A0623	Putative tRNA -methyltransferase	3.57	2.78

[1] FC: fold-change. *i.e.* NSAF ratio VAR-F48 vs WT

Table 3: Exoproteins for which differential accumulation was measured in VAR-F48 compared to WT after 24 h and/or 72 h incubation in groundwater.

Uniprot-ID	Gene	ORF	Description	$Log_2(FC)$[1]	
				T1	T2
Carbohydrate transport and metabolism					
B7HW93	tal	BCAH187_A0799	Probable transaldolase	NS	-4.55
Coenzyme transport and metabolism					
B7HPS6	pdxS	BCAH187_A0016	Pyridoxal 5'-phosphate synthase	4.08	NS
Posttranslational modification. protein turnover. chaperones					
B7HN40		BCAH187_A4193	Peptidyl-prolyl cis-trans isomerase	4.80	NS
Secondary metabolite biosynthesis. transport and catabolism					
B7HZW9		BCAH187_A3546	Glyoxalase family protein	NS	-3.77
Translation. ribosomal structure and biogenesis					
B7HQU4	rplC	BCAH187_A0141	50S ribosomal protein L3	NS	-4.47
B7HQV6	rplE	BCAH187_A0153	50S ribosomal protein L5	NS	-4.74
B7HQV9	rplF	BCAH187_A0156	50S ribosomal protein L6	NS	-4.47
B7HQV4	rplN	BCAH187_A0151	50S ribosomal protein L14	NS	-3.94
B7HLH3	rplS	BCAH187_A3887	50S ribosomal protein L19	NS	-6.04
B7HRL2	rplT	BCAH187_A4697	50S ribosomal protein L20	NS	-5.26
B7HQK2	rplU	BCAH187_A4577	50S ribosomal protein L21	NS	-4.49
B7HQU6	rplW	BCAH187_A0143	50S ribosomal protein L23	NS	-5.79
B7HSJ2	rpsD	BCAH187_A4790	30S ribosomal protein S4	NS	-4.24

[1] FC: fold-change. *i.e.* NSAF ratio VAR-F48 vs WT; NS: Not significant.

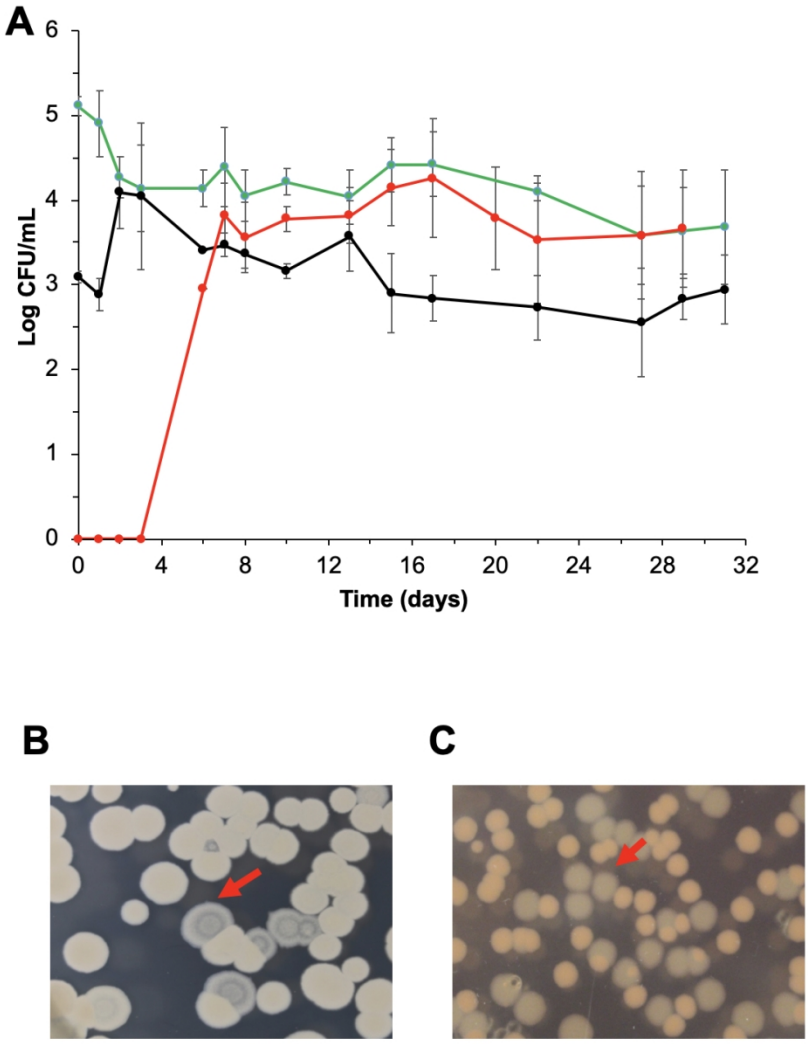

Figure 1

Figure 1

208x288mm (144 x 144 DPI)

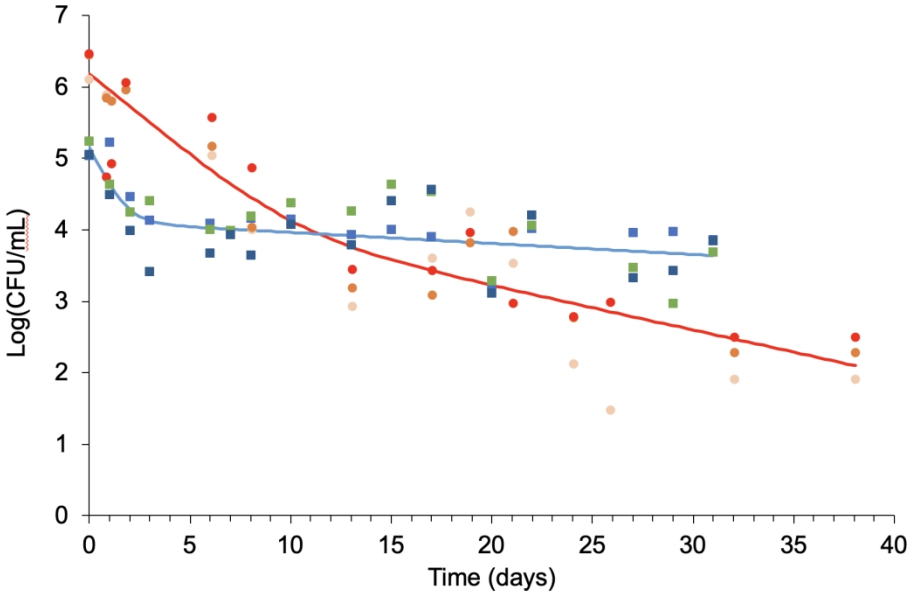

Figure 2

344x238mm (144 x 144 DPI)

A

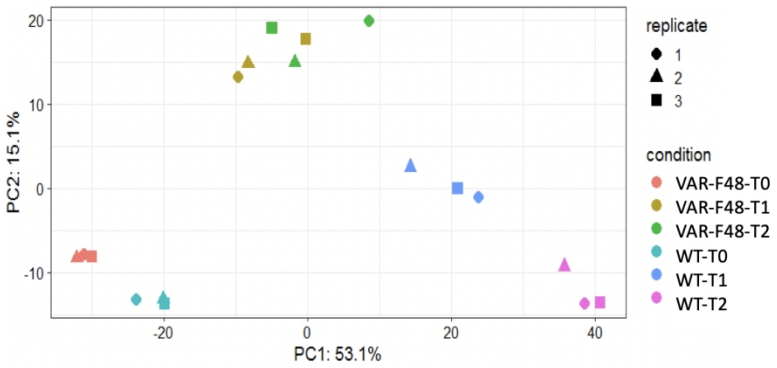

B

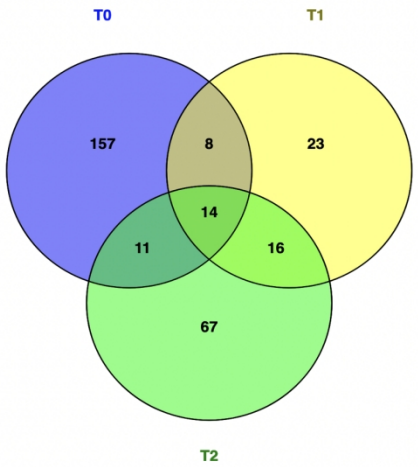

Figure 3

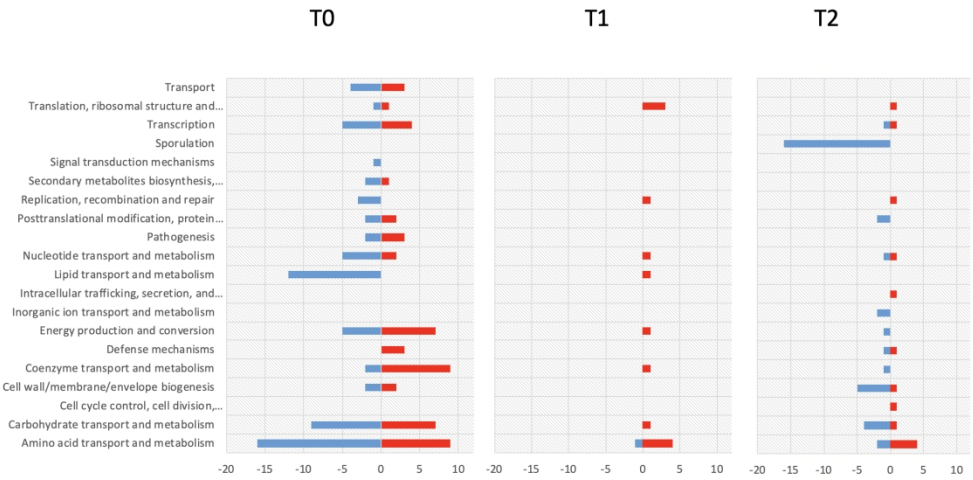

Figure 4

Figure 4

431x267mm (144 x 144 DPI)

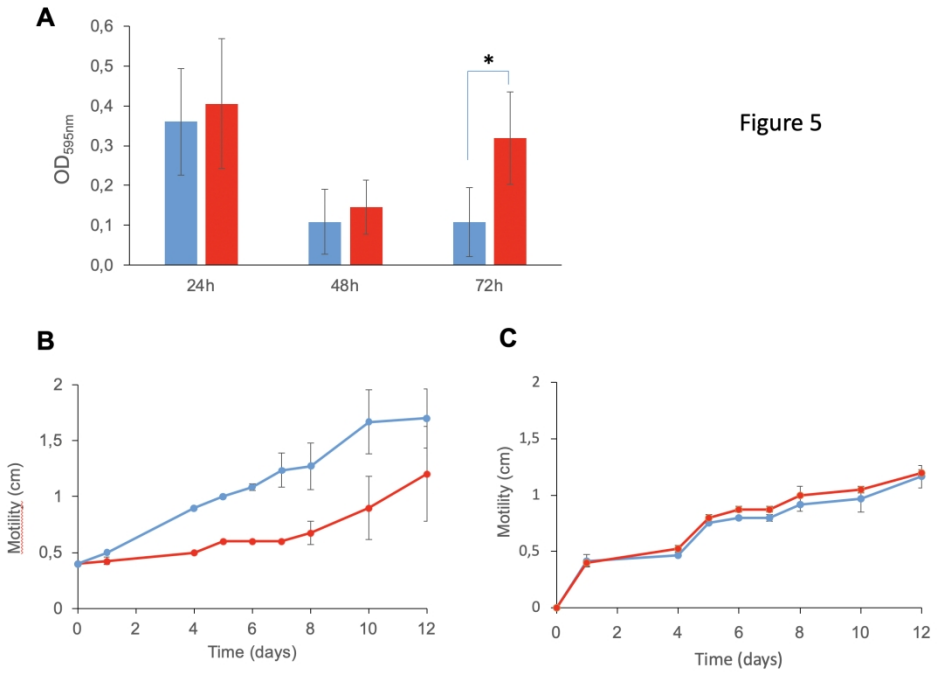

Figure 5

Figure 5

424x306mm (144 x 144 DPI)

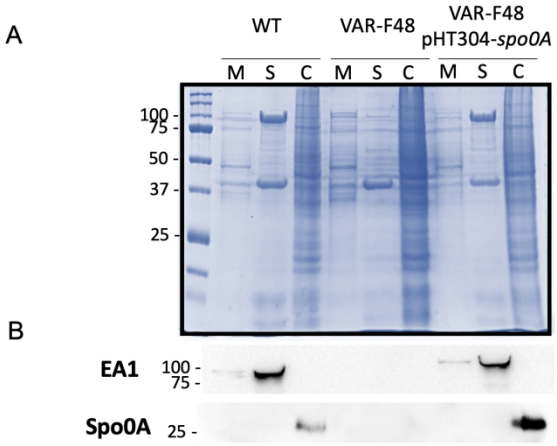

Figure 6

Figure 6

438x268mm (144 x 144 DPI)